Chemistry and Physics of Lipids 223 (2019) 104784

Contents lists available at ScienceDirect

Chemistry and Physics of Lipids

journal homepage: www.elsevier.com/locate/chemphyslip

Behavior of the DPH fluorescence probe in membranes perturbed by drugs

Chetan Poojari[a], Natalia Wilkosz[b], Rafael B. Lira[c], Rumiana Dimova[c], Piotr Jurkiewicz[d], Rafał Petka[b], Mariusz Kepczynski[b,**], Tomasz Róg[a,e,*]

[a] Department of Physics, Tampere University of Technology, PO Box 692, FI-33101 Tampere, Finland
[b] Faculty of Chemistry, Jagiellonian University, Gronostajowa 2, 30-387, Kraków, Poland
[c] Max Planck Institute of Colloids and Interfaces, Science Park Golm, 14424, Potsdam, Germany
[d] J. Heyrovský Institute of Physical Chemistry AS CR, v.v.i, Dolejškova 2155/3, 182 23 Prague 8, Czech Republic
[e] Department of Physics, University of Helsinki, PO Box 64, FI-00014, Helsinki, Finland

ARTICLE INFO

Keywords:
1,6-diphenyl-1,3,5-hexatriene
Lipid bilayers
Molecular dynamics simulations
Fluorescence anisotropy

ABSTRACT

1,6-Diphenyl-1,3,5-hexatriene (DPH) is one of the most commonly used fluorescent probes to study dynamical and structural properties of lipid bilayers and cellular membranes via measuring steady-state or time-resolved fluorescence anisotropy. In this study, we present a limitation in the use of DPH to predict the order of lipid acyl chains when the lipid bilayer is doped with itraconazole (ITZ), an antifungal drug. Our steady-state fluorescence anisotropy measurements showed a significant decrease in fluorescence anisotropy of DPH embedded in the ITZ-containing membrane, suggesting a substantial increase in membrane fluidity, which indirectly indicates a decrease in the order of the hydrocarbon chains. This result or its interpretation is in disagreement with the fluorescence recovery after photobleaching measurements and molecular dynamics (MD) simulation data. The results of these experiments and calculations indicate an increase in the hydrocarbon chain order. The MD simulations of the bilayer containing both ITZ and DPH provide explanations for these observations. Apparently, in the presence of the drug, the DPH molecules are pushed deeper into the hydrophobic membrane core below the lipid double bonds, and the probe predominately adopts the orientation of the ITZ molecules that is parallel to the membrane surface, instead of orienting parallel to the lipid acyl chains. For this reason, DPH anisotropy provides information related to the less ordered central region of the membrane rather than reporting the properties of the upper segments of the lipid acyl chains.

1. Introduction

Free fluorescent probes and labels are commonly used in the studies of biological systems at both cellular and molecular levels. Model lipid bilayers or biological membranes are no exception here. Fluorescent probes are very useful to monitor the lipid tail order, hydration at the membrane-water interface, membrane electrostatic properties, and dynamics of membrane components, such as diffusion or relaxation processes (Demchenko et al., 2009; Klymchenko and Kreder, 2014). However, molecular probes or labels are unnatural elements of the studied systems. Thus, the important question is how much the presence of the probe affects the membrane properties and how much the behavior of the probe reflects the behavior of the unmodified membranes. In recent years, molecular dynamics (MD) simulations have been used to understand the behavior of fluorescent probes, thereby facilitating the interpretation of experimental data and providing detailed information on the location and orientation of the probes, and their impact on surrounding lipid molecules (Faller, 2016; Kepczynski and Róg, 2016). Recent studies include, e.g., NBD-labeled lipids (Filipe et al., 2014), F2N12S (Timr et al., 2015), and ATTO647N, ATTO532, KK114 (Mobarak et al., 2018).

1,6-Diphenyl-1,3,5-hexatriene (DPH) is a probe extensively used to determine the structural and dynamical features of lipid bilayers. In particular, DPH fluorescence anisotropy is a parameter interpreted as a membrane microviscosity (viscosity in the bilayer interior) or fluidity. Interpretation of the fluorescence anisotropy is not straightforward as it provides information about the orientation and dynamics of the probe in the lipid bilayer. Recent examples of the application of DPH to investigate model lipid bilayers include comparative studies of the effect of cholesterol (Chol) and its analogues (cholesteryl hemisuccinate (Kulig et al., 2015a), oxysterols (Gomes et al., 2018; Kulig et al., 2015b), lanosterol, and ergosterol (Bui et al., 2016) on the bilayer

* Corresponding author at: Department of Physics, University of Helsinki, PO Box 64, FI-00014, Helsinki, Finland
** Corresponding author at: Faculty of Chemistry, Jagiellonian University, Gronostajowa 2, 30-387, Kraków, Poland.
E-mail addresses: kepczyns@chemia.uj.edu.pl (M. Kepczynski), tomasz.rog@gmail.com (T. Róg).

https://doi.org/10.1016/j.chemphyslip.2019.104784
Received 26 January 2019; Received in revised form 9 May 2019; Accepted 8 June 2019
Available online 12 June 2019

properties. Other examples include the reorganization of cholesterol-rich bilayers due to the addition of polyunsaturated fatty acids (Mason et al., 2016), α-synuclein peptides (Pirc and Ulrih, 2015), and interactions of amyloid β-peptide with lipid bilayers (Suzuki and Miura, 2015), interactions of dendrimers with artificial bilayers and monolayers (Melikishvili et al., 2016), or toxin-induced pore formation (García-Linares et al., 2016). DPH is also frequently used to study the effect of drugs and drug-like small molecules on lipid bilayer properties (Alves et al., 2017; Balducci et al., 2018; De Athayde et al., 2016; dos Santos et al., 2017; Giudice et al., 2016; Miguel et al., 2018; Neves et al., 2016, 2015; Vaňousová et al., 2018; Yun and Lee, 2017; Yun et al., 2015). The use of DPH is not limited to model bilayer studies, intact biological membranes are also investigated using the DPH probe (Brejchová et al., 2015; Cerecedo et al., 2016; Wang et al., 2018, 2016; Yun et al., 2018).

The effects of DPH on lipid bilayers has been investigated using experimental and MD simulations methods. Repáková et al. used differential scanning calorimetry, ^{2}H NMR measurements, and atomistic MD simulations to study the behavior of DPH embedded in the saturated (1,2-dipalmitoyl-*sn*-glycero-3-phosphocholine, DPPC) bilayer in the liquid-crystalline phase (Repáková et al., 2005, 2004). They found that the probe slightly increases the lipid acyl tail order in the DPPC bilayer and has a weak effect on the DPPC phase transition. In the case of the mixed DPPC/Chol (5 and 20 mol %) bilayer, it was shown by MD simulations that DPH affects the membrane properties, but the DPH-induced perturbations are local and depend on the concentration of Chol in the membrane (Fraňová et al., 2010). Recently, MD simulations of DPH behavior in the 2-oleoyl-1-palmitoyl-*sn*-glycero-3-phosphocholine (POPC) and POPC/Chol bilayers were performed (do Canto et al., 2016). These studies showed a weak ordering effect of the probe on the POPC bilayer, with the ordering being stronger at the end of the acyl tails. The effect of DPH on the POPC/Chol bilayer was even weaker; only the segments at the beginning of the acyl tail were slightly disordered.

In this study, we employed atomic-scale MD simulations combined with steady-state fluorescence anisotropy and fluorescence lifetime measurements and fluorescence recovery after photobleaching (FRAP) experiments to evaluate the usefulness of the DPH probe as a reporter on the properties of zwitterionic membranes doped with a hydrophobic drug. We used itraconazole (ITZ) as a model hydrophobic drug. ITZ is an orally administered triazole antifungal agent frequently used to treat severe mycotic infections in both regular and immunocompromised patients (Clissold and Grant, 1989). First, the effect of ITZ on the properties of the POPC bilayer was examined. Next, we compared the behavior of DPH in the pristine and ITZ-doped POPC bilayer. Our results show that the location and orientation of DPH is strongly affected by the drug molecules that adopt an orientation parallel to the membrane surface.

2. Materials and methods

2.1. Materials

Itraconazole (ITZ), synthetic 1-palmitoyl-2-oleoyl-*sn*-glycero-3-phosphocholine (POPC), 2,2′-(1,4-phenylene)bis[5-phenyl-oxazole] (POPOP), sucrose, and glucose were purchased from Sigma-Aldrich. 1,6-Diphenyl-1,3,5-hexatriene (DPH, for fluorescence, ≥97.5%) was received from Fluka. 1,2-Dipalmitoyl-*sn*-glycero-3-phosphoethanolamine-*N*- (lissamine rhodamine B sulfonyl) (DPPE-Rh) was purchased from Avanti Polar Lipids (Alabaster, AL). Low gelling temperature agarose was purchased from Fisher Scientific (Waltham, MA). All solvents were obtained from Aldrich. Dimethylformamide (DMF) was of spectroscopic grade. Milipore-quality water was used during the experiments.

2.2. Preparation of liposomes

POPC/ITZ small unilamellar vesicles (SUVs) were prepared by sonication as described previously (Kepczynski et al., 2010). Briefly, stock solutions of POPC (34.6 mM) and ITZ (9.5 mM) were prepared in chloroform. Appropriate volumes of the stock solutions were combined in a volumetric flask, and then the solvent was evaporated under a stream of nitrogen to complete dryness. The dry film was hydrated with 10 mM phosphate buffer pH 7.4. The final concentration of POPC was 2.5 mg/mL. The size of POPC/ITZ liposomes was in the range of 30–200 nm (Dzieciuch-Rojek et al., 2017). Giant unilamellar vesicles (GUVs) were prepared by electroformation (Lira et al., 2014), see also (Dimova, 2019). A stock solution containing 3 mM of POPC and 0.5 mol % of DPPE-Rh was prepared in chloroform and mixed with appropriate volumes of the ITZ stock solution. Ten μL of the solution were spread on a pair of conductive glasses coated with indium tin oxide. The solvent was evaporated under a stream of nitrogen for 5 min. The glasses were sandwiched using a 1 mm Teflon spacer, forming a 1.5 ml chamber. A 0.2 M sucrose solution was added to the chamber to hydrate the lipid films and the chamber was connected to a function generator. A 10 Hz AC field of 1 V amplitude was applied, and the vesicles were allowed to grow for 1 h at room temperature in the dark. The vesicles were harvested and dispersed in an isotonic glucose solution for subsequent imaging and analysis.

2.3. Steady-state fluorescence anisotropy measurements

DPH was dissolved in DMF to form a stock solution. The POPC/ITZ liposomes were stained with DPH in the dark for 1 h. The final concentration of DPH was 1.02×10^{-7} M. Anisotropy measurements were performed as described previously (Kepczynski et al., 2011) using an SLM-AMINCO 8100 spectrofluorimeter working in the L-format and equipped with automatic polarizers. Samples were excited at $\lambda_{exc} = 350$ nm and the fluorescence intensity was monitored at $\lambda_{em} = 428$ nm. The steady state anisotropy (r) was calculated using the following equation (Lakowicz, 2006):

$$r = \frac{I_{vv} - GI_{vh}}{I_{vv} + 2GI_{vh}} \quad (1)$$

where I is the fluorescence intensity, 'v' and 'h' subscripts denote the vertical and horizontal settings of the excitation and emission polarizers, respectively. G is an instrumental correction factor and was calculated individually for each sample according to the equation:

$$G = \frac{I_{hv}}{I_{hh}} \quad (2)$$

The apparent microviscosity was calculated using Eq. (3) (Pandey and Mishra, 1999).

$$\bar{\eta} = \frac{2.4r}{0.362 - r} \quad (3)$$

2.4. Fluorescence lifetimes of DPH

All fluorescence measurements were performed in 1.5 ml quartz cuvettes. The temperature of (293 ± 0.5) K was maintained using a water-circulating thermostat. Samples were equilibrated for 10 min before each measurement. Steady-state fluorescence spectra was collected using a Fluorolog-3 spectrofluorimeter (model FL3-11, JobinYvon Inc., Edison, NJ, USA). Fluorescence decays were recorded on a time-correlated single-photon counting (TCSPC) spectrometer, model 5000 U SPC, equipped with a 375 nm NanoLED 11 diode laser and a cooled Hamamatsu R3809U-50 microchannel plate photomultiplier (IBH, Glasgow, UK). The excitation and emission wavelengths (EX/EM = 375/466 nm) were chosen using monochromators and a 399 nm cut-off filter was used to eliminate scattered light. The

global fitting of the fluorescence decays were performed using FluoFit v.4.5 (PicoQuant, Berlin, Germany), as described in the Supplementary Materials.

2.5. Fluorescence recovery after photobleaching (FRAP)

FRAP experiments were performed as described previously (Lira et al., 2016) using a Leica TCS SP8 (Wetzlar, Germany) microscope with a 63× (1.2 NA) water immersion objective and an 1 Airy unit. A 561 nm diode-pumped solid-state laser was used for excitation. DPPE-Rh-labeled GUVs were immobilized by dilution in 0.1% w/v agarose according to the previously reported protocol (Lira et al., 2016). Photobleaching was performed using the 561 nm laser in a circular region of interest (ROI) with a nominal radius of $r_n = 3\,\mu m$. The laser was then switched back to the attenuated intensity and the recovery images were recorded for several seconds. Photobleaching was performed on the upper or lower pole of the GUVs. Data were analyzed according to a simplified equation considering molecular diffusion during photobleaching, hence reducing error. The diffusion coefficient, D, is given as (Kang et al., 2012):

$$D = \frac{r_e^2 + r_n^2}{8t_{1/2}} \tag{4}$$

where r_e and r_n are the effective and nominal (i.e., user-defined) bleaching radii and $t_{1/2}$ is the half-time of fluorescence recovery (i.e., the time to reach $F_{1/2} = (F_o + F_\infty)/2$, where F_o and F_∞ are the fluorescence intensity in the first post-bleach image and after full recovery, respectively). To obtain r_e, the fluorescence intensity line profile $f(x)$ through the center of the bleaching spot in the first post-bleaching image was fitted with the expression

$$f(x) = 1 - Ke^{-\frac{2x^2}{r_e^2}} \tag{5}$$

where K is the bleaching depth.

2.6. MD simulations

Atomistic MD simulations were performed for the following model systems (see Table 1): (1) the pure POPC bilayer (system **POPC**), (2) the POPC bilayer labeled with 1.5 mol% of DPH (system **DPH-POPC**), (3) the POPCeq bilayer containing 9 mol% ITZ (system **ITZ-POPC**), and (4) the POPC bilayer doped with 9 mol% of ITZ and 1.4 mol% of DPH (system **ITZ/DPH-POPC**). Images of the initial and final configurations are shown in Fig. 1.

To parameterize POPC, ITZ, DPH, and ions, we used the all-atom OPLS force field (Kaminski et al., 2001). Additional force field parameters specifically derived and validated for lipids can be found in our previous papers (Kulig et al., 2016, 2015c; Maciejewski et al., 2014). Partial charges for ITZ are taken from our previous studies (Dzieciuch-Rojek et al., 2017). For water, we used the TIP3P model that is compatible with the OPLS-AA force field (Jorgensen et al., 1983). Partial charges for DPH were derived in accordance with the OPLS-AA methodology, and are given in supplementary materials as a part of the topology file in the GROMACS format.

All the systems were fully hydrated and the physiological salt concentration was introduced. Prior to MD simulations, the initial configurations were energy minimized using the steepest-descent algorithm. Next, the systems were equilibrated under NVT conditions with position restraints applied on the lipid phosphorus atom and ITZ/DPH molecules. The v-rescale method was used to couple the temperature at 300 K with separate heat baths for the membrane, and the rest with time constants of 0.1 ps (Bussi et al., 2007). Following NVT equilibration, the systems were equilibrated under NPT conditions and the position restraints applied in the NVT step were gradually removed. The reference pressure was set to 1 bar and coupled to the semi-isotropic Parrinello–Rahman barostat (Parrinello and Rahman, 1981). For the long-range electrostatic interactions, the particle-mesh Ewald (PME) method was used (Darden et al., 1993; Essmann et al., 1995), with real space cut-off 1 nm. Lennard-Jones interactions cut-off was 1 nm. The covalent bond lengths were preserved using the linear constraint solver (LINCS) algorithm (Hess et al., 1997).

The final production MD simulations were carried without any position restraints, and the input parameters were the same as those used during the NPT run. The time step was set to 2 fs, and the simulations were carried out using the GROMACS 4.5 software package (Pronk et al., 2013). The analyses were performed for the last 250 ns for the systems containing DPH and ITZ and the last 150 ns in the case of system **POPC**.

Table 1
Summary of simulated systems. For each system, the table indicates the number of molecules in the given system and the simulation time.

System	POPC	ITZ	DPH	Water	Na^+/Cl^-	Simulation length (ns)
POPC	1024	–	–	76014	206	250
DPH-POPC	1024	–	16	69775	189	1000
ITZ-POPC	1024	102	–	76014	206	500
ITZ/DPH-POPC	1024	102	16	74431	202	1000

3. Results

3.1. Steady-state fluorescence anisotropy of DPH

We studied the effect of the ITZ mole fraction (X_{ITZ}) on fluorescence anisotropy (r) of DPH embedded into the POPC/ITZ membrane of SUVs. Fig. 2 shows that the value of r decreases with increasing ITZ concentration in the mixed POPC/ITZ membrane.

The DPH fluorescence anisotropy can be reduced due to rotational diffusion, which is a function of the environment microviscosity. The apparent microviscosities were calculated from the measured anisotropies using the Perrin equation (Eq. (3)) and are listed in Table S1. The values suggest that the addition of ITZ leads to a reduction in the microviscosity of the lipid bilayer, therefore freedom of rotational motion of the rigid molecular probe should increase, indicating an increase in the bilayer fluidity with increasing drug concentration.

3.2. Fluorescence lifetime of DPH

We measured the fluorescence lifetimes of DPH embedded in the POPC and POPC/ITZ ($X_{ITZ} = 0.2$) liposomes by single photon counting techniques (Fig. S2, the Supplementary Materials). For both systems, the best fit for fluorescence decays was obtained using a two-exponential model (Table 2), which shows that DPH has two fluorescence lifetimes, when it is incorporated into lipid membranes. Our results are in line with the literature values. The DPH lifetime values obtained for the pure POPC membrane are typical for those reported for lipid membranes being in the liquid-crystalline state. However, the incorporation of ITZ into the POPC membrane results in an increase in the values of both lifetimes. It has been shown that, depending on the composition and physical state of the membrane, the fluorescence decay of DPH in the lipid membranes is characterized by a long-lifetime component (with a higher fractional intensity), whose lifetime can vary within the 7–10.5 ns range, and a short-lifetime component (with a lower fractional intensity) of lifetimes in the range of 1–3 ns (Fiorini et al., 1987). In general, DPH lifetimes are longer in more ordered membranes (e.g., in the gel state). In addition, it is well-known that the DPH lifetime is highly sensitive to the polarity (dielectric constant) of the medium in which it is embedded, and it is much shorter in polar environments (Zannoni et al., 1983). The polarity (hydrophobicity) of phospholipid bilayers is depth-dependent and is largely determined by the extent of water penetration into the membrane (Kepczyński et al.,

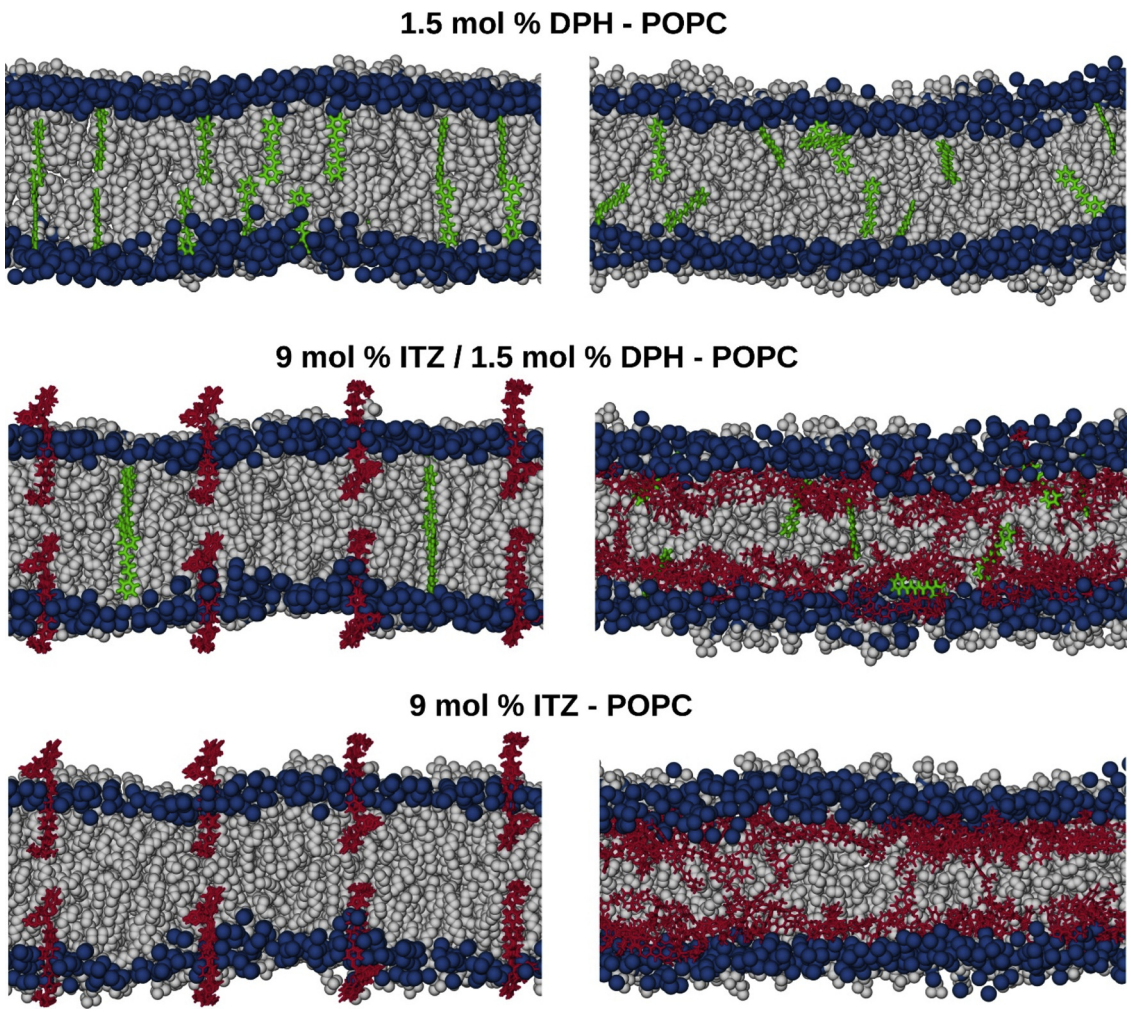

Fig. 1. Initial and final configurations for model systems (**DPH-POPC**, **ITZ/DPH-POPC**, and **ITZ-POPC**) are shown on the left and right panels, respectively. POPC phosphate atoms and acyl chains are shown as blue and gray spheres, respectively. DPH is shown in green and ITZ in red. Water and ions are not shown for clarity.

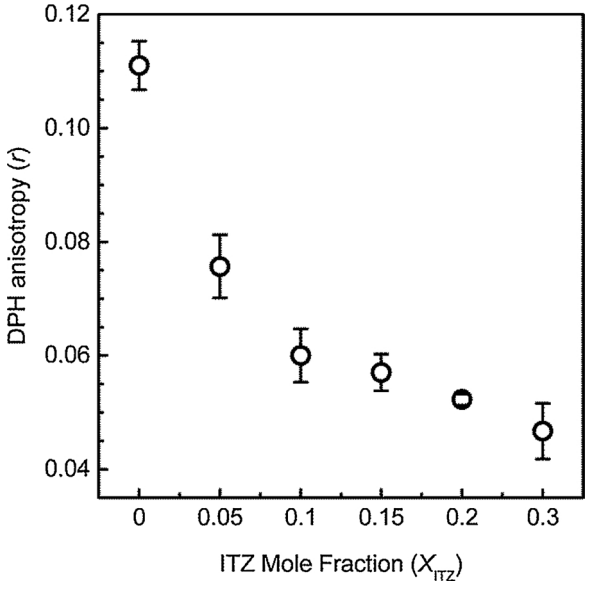

Fig. 2. The effect of the ITZ mole fraction on the fluorescence anisotropy of the DPH probe incorporated into the POPC/ITZ bilayer (λ_{exc} = 350 nm, λ_{em} = 428 nm, $c_{DPH} = 1.02 \times 10^{-7}$ M). Values are the mean of three independent experiments and the error bars correspond to the standard deviations.

Table 2
Fluorescence lifetime of DPH embedded into POPC and POPC/ITZ (X_{ITZ} = 0.2) liposomes.

System	τ_1 [ns]	α_1	τ_2 [ns]	α_2
POPC	8.38 ± 0.03	0.89	2.35 ± 0.32	0.11
POPC/ITZ	9.03 ± 0.02	0.80	3.08 ± 0.13	0.20

2008). Therefore, we believe that the observed increase in the DPH lifetimes in the presence of the drug may be the result of a deeper location (less accessible to water) of the probe and/or a drug-induced increase in the ordering of the POPC membrane.

3.3. The effect of ITZ on dynamics of POPC molecules in the bilayer

To verify whether ITZ can increase the fluidity of lipid membranes, we focused on the dynamics of lipid molecules in the POPC membrane of GUVs. The lateral diffusion coefficients (D_L) of DPPE-Rh in the POPC bilayer doped with ITZ (X_{ITZ} varied between 0.0 to 0.2) were calculated from the FRAP measurements. Fig. 3 shows the changes of the diffusion coefficient with increasing ITZ concentration. The average D_L values are also shown in Table S1. Our data for the diffusivity of DPPE-Rh in the pure bilayer are in good agreement with the NMR studies of POPC diffusion that reported the lateral diffusion coefficient for the lipid of 1.4×10^{-7} cm^2/s at 308 K and 1.9×10^{-7} cm^2/s at 313 K (Filippov et al., 2003). A comparable diffusion coefficient value for the POPC

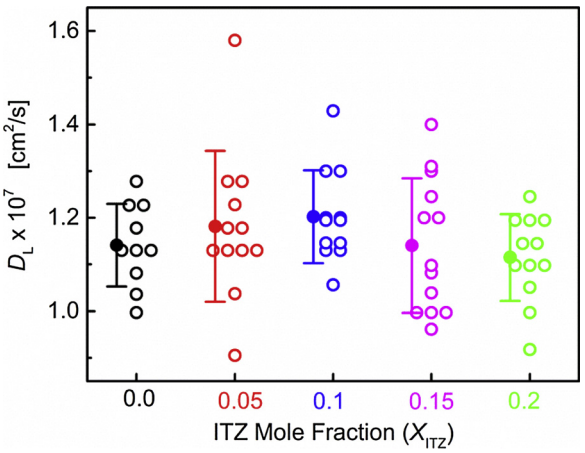

Fig. 3. Diffusion coefficient (D_L) of DPPE-Rh in POPC GUVs as a function of ITZ molar fraction in the membrane. Each point (open circles) represents a single FRAP measurement on an individual GUV and the mean values (solid circles) with standard deviations for each X_{ITZ} are depicted. The POPC/ITZ GUVs were labeled with 0.5 mol% DPPE-Rh.

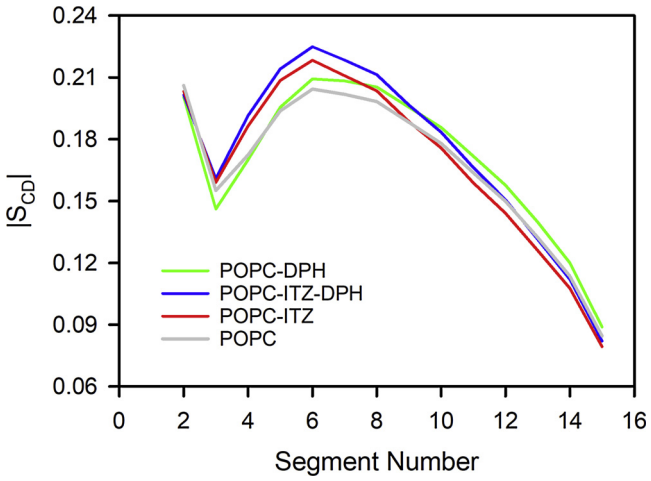

Fig. 4. Profiles of the molecular order parameter $|S_{CD}|$ of the *sn*-1 acyl tail of POPC in systems **POPC** (orange line), **DPH-POPC** (green line), **ITZ/DPH-POPC** (blue line), and **ITZ-POPC** (red line).

molecules, DL = (1.68 ± 0.04) × 10^{-7} cm^2/s, was obtained using MD simulations (Stepniewski et al., 2012). The results for the mixed ITZ/POPC membranes demonstrated that the effect of ITZ on the lipid dynamics in the membrane is rather limited. We observed a slight increase in the D_L value after inclusion up to 10 mol% ITZ, but a further increase in the ITZ content resulted in a reduction of the DPPE-Rh diffusion coefficient.

3.4. Molecular insight into the effect of DPH and ITZ on the bilayer properties

To describe the structure of the lipid bilayers, we used three standard parameters: area per lipid molecule (*APL*), membrane thickness and molecular order parameter (S_{CD}). *APL* was obtained by dividing the area of the simulation box in the membrane plane by the number of lipid molecules in a single bilayer leaflet, while the membrane thickness was approximated by measuring the distance between the average positions of phosphorus atoms in the opposite leaflets (the P-P distance). Values of *APL* and thickness are given in Table 3. The *APL* value calculated for the pure POPC bilayer is the same as that obtained previously experimentally (0.64 ± 0.01 nm^2 at 25 °C) (König et al., 1997).

The S_{CD} parameter is defined as follows:

$$S_{CD} = \left\langle \frac{3}{2}(\cos^2\theta_i) - \frac{1}{2} \right\rangle, \quad (6)$$

where θi is the angle between the C–D bond (C–H in simulations) of the *i*-th carbon atom and the bilayer normal. The angular brackets denote averaging over time and relevant C–D bonds in the bilayer. The profiles of the S_{CD} parameter along the *sn*1 tail of POPC are shown in Fig. 4. The incorporation of 1.5 mol % of DPH had a little impact on the organization of the POPC membrane. The ordering of the saturated acyl chains slightly increased, which caused an increase in the membrane thickness (0.1 nm), while the *APL* was remained unchanged. In contrast, the presence of ca. 9 mol% of ITZ significantly changed the membrane organization, and the impact of the drug was different for the different hydrocarbon segments. We observe a considerable increase in the ordering of the carbon atoms near the hydrophilic region (C3-C6 carbon atoms) and a reduction in the ordering of the carbon atoms located in the center of the membrane (C8-C15 carbon atoms). These changes were accompanied by a significant increase in the *APL* (0.07 nm^2). The most pronounced changes in the membrane organization were observed for the system containing both the probe and the drug. Introduction of DPH to the ITZ-POPC bilayer led to a significant increase in the ordering along the whole hydrocarbon chain, which was accompanied by an increase in the bilayer thickness.

Table 3
Values of Area per Lipid (*APL*) and Bilayer Thickness. Errors for *APL* are less than 0.005 nm^2 and for Thickness less than 0.04 nm.

Bilayer	*APL* [nm^2]	Thickness [nm]
POPC	0.64	3.7
DPH-POPC	0.64	3.8
ITZ-POPC	0.71	3.7
ITZ/DPH-POPC	0.71	3.8

3.5. DPH and ITZ behavior in the POPC membrane

We calculated mass density profiles to describe the locations of DPH and ITZ in the lipid bilayers. Fig. 5 shows that the ITZ molecules locate below the lipid headgroups and slightly above the double bonds of the *sn*2 (oleyl) hydrocarbon chains of POPC, see also Fig. 1. This location was not affected by the presence of DPH and agrees with our previous studies (Dzieciuch-Rojek et al., 2017). On the contrary, the location of DPH molecules was dependent on the presence of ITZ in the membrane. The maximum of DPH distribution was shifted by about 0.4 nm towards the center of bilayer after the drug incorporation. Thus, in the presence of the drug, the DPH molecules were pushed deeper into the hydrophobic membrane core below the lipid double bonds.

To describe the orientations of the ITZ and DPH molecules in the POPC bilayer, we calculated the distributions of the angle between the rigid vectors defined for the molecules, shown as red and blue arrows in Fig. 6, and the bilayer normal. It is not surprising that the presence of DPH did not affect the orientation of ITZ molecules. On the contrary, the impact of ITZ on the DPH orientation was substantial. The DPH molecules adopted an orientation similar to that for ITZ and were aligned more perpendicular to the bilayer normal (parallel to the membrane surface).

4. Discussion

DPH is the most commonly applied rotational probe for estimating microviscosity and fluidity of lipid membranes in the acyl chain region (Kepczyński et al., 2008). In our previous studies, we have obtained consistent results on the properties of membranes composed of different lipids using DPH anisotropy measurements and MD simulations (Kulig et al., 2015a, 2015b). More specifically, the increase/decrease in the

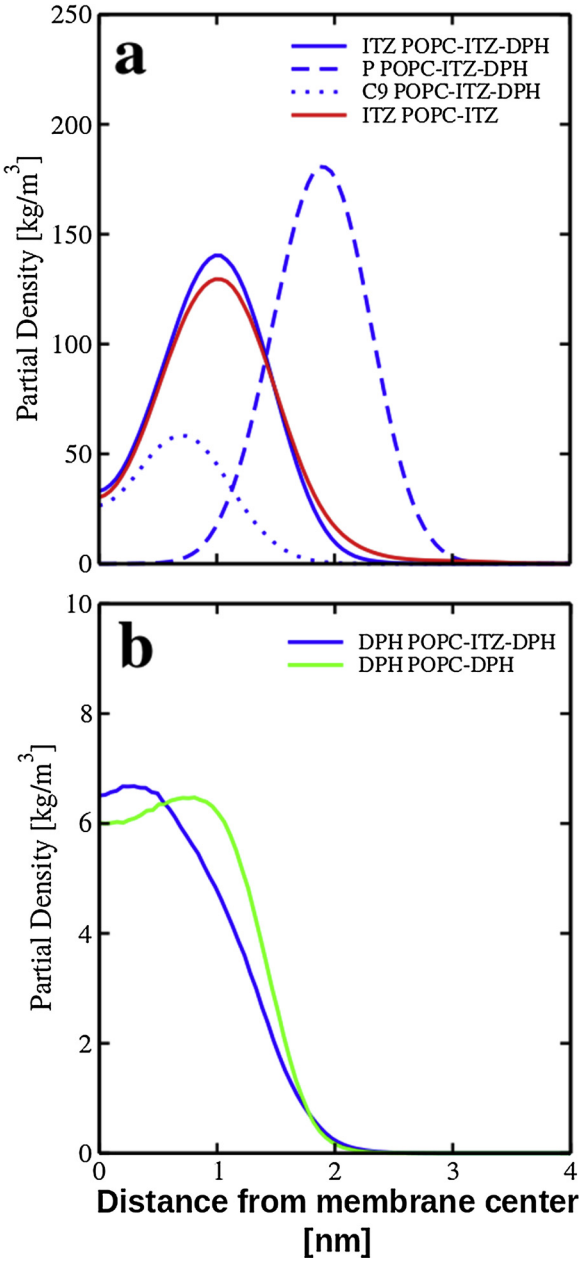

Fig. 5. (a) Mass density profiles of ITZ in systems **ITZ/DPH-POPC** (blue line) and **ITZ-POPC** (red line), and phosphates (dashed-blue line) and double bonds of the POPC *sn*2 chain (doted-blue line) in system **ITZ/DPH-POPC**. (b) Mass density profiles of DPH in the systems **ITZ/DPH-POPC** (blue line) and **DPH-POPC** (green line) bilayers. The plots were averaged over both bilayer leaflets.

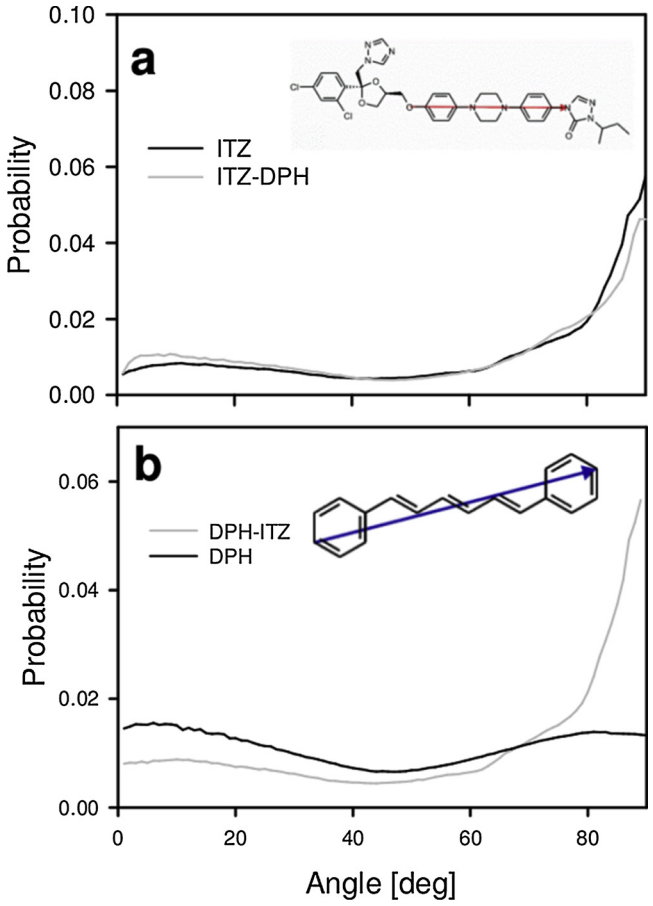

Fig. 6. Distribution of the angle between (a) ITZ and (b) DPH long axis and the bilayer normal in ITZ/DPH-POPC (gray lines), DPH-POPC and ITZ-POPC (black lines) bilayers. Structures of a (2R,4S) stereoisomer of ITZ and DPH depicting the vectors (red and blue arrows) of their principal axes that define the molecule key orientations are shown as insets.

order of lipid tails observed in the MD simulations was in qualitative agreement with the increase/decrease in steady-state fluorescence anisotropy. In this article, we consider the utility of the DPH probe as a reporter on the properties of biomembranes modified by the presence of the hydrophobic drug. For this purpose, we first examined the effect of ITZ on the POPC membrane. Next, we compared the behavior of DPH in the pure and ITZ-doped POPC bilayer.

4.1. ITZ increases the free volume of the POPC membrane, but has little effect on lipid dynamics

Our MD simulations show that the rod-like ITZ molecules are preferentially localized in the region of the upper segments of the lipid acyl tails, close to the headgroups, as depicted in Fig. 1, and are oriented mostly parallel to the membrane surface (Fig. 6a). Such location and orientation of the drug molecules considerable affect the arrangements of lipid molecules in the membrane. As indicated by the increase in *APL* (Table 3), the presence of the drug causes the lipid molecules to move apart from each other. In addition, ITZ increases the order of the upper segments of the acyl chains close to the carbonyl groups (C2-C6 carbon atoms) and reduces the ordering for the segments below the 9th carbon atoms in the bilayer (Fig. 4). As a consequence, the free volume (the unoccupied volume enclosed in the bilayer) between the POPC molecules considerably increases in the deeper part of the membrane. The experimental results are consistent with the MD simulations. The direct measurements of the lateral diffusion of lipid molecules in the mixed POPC/ITZ membrane (Fig. 3) reveal that the drug has little influence on lipid motility; thus, the incorporation of ITZ into the zwitterionic membranes does not affect membrane fluidity.

4.2. The DPH probe has a negligible impact on the membrane order and packing

The MD simulations demonstrate that the incorporation of up to 1.5 mol% of the probe into the POPC membrane (system **DPH-POPC**) has the negligible effect on the ordering and packing of the lipid acyl chains in the bilayer. These findings agree with previous MD simulations of much smaller systems (128 POPC molecules) doped with ca. 1.5 and 3.1 mol% of DPH (do Canto et al., 2016). The incorporation of the smaller amount did not affect the *APL* and slightly increased the membrane thickness and the ordering of the lipid acyl chains compared

to the pure bilayer.

4.3. ITZ has a considerable effect on the location and orientation of DPH probe in the membrane

Knowledge of the position and orientation of molecular probes in membranes is essential to understand the information obtained with their help. To study the behavior of DPH in the unsaturated bilayer, we performed MD simulations. The mass density profile for DPH in the POPC membrane is broad, with a maximum at ca. 0.79 nm from the membrane center. This value is almost the same as that determined experimentally by Kaiser and London (Kaiser and London, 1998), who investigated the transverse distribution of DPH within the 1,2-dioleoyl-sn-glycero-3-phosphocholine (DOPC) bilayer using the parallax method. The average distance of the center of the fluorophore molecule from the center of the bilayer was estimated to be 0.78 nm. Using MD simulations, Repakova et al. showed that the average position of DPH in the DPPC membrane is about 0.75 nm, although the position distribution is rather broad, extending from 0.3 nm to 1.3 nm (Repáková et al., 2004). It is noteworthy that DPH can also penetrate the bilayer center, as the distribution profile is non-zero at the membrane center (depth of 0).

Our simulations show that the orientational distribution of DPH is bimodal (Fig. 6) with a population of molecules that almost align with the bilayer normal or orient parallel to the bilayer surface. This result differs from previous studies, in which the DPH molecules were found to arrange parallel to the bilayer normal in bilayers from saturated lipids (Repáková et al., 2005, 2004) or bilayers made of saturated and unsaturated lipids mixed with cholesterol (do Canto et al., 2016; Fraňová et al., 2010). However, the bimodal distributions of the long axis of the probe, indicating fractions of the probe molecules oriented parallel and perpendicular to the preferred direction of the lipids, were shown for DPH embedded in liposomes made of saturated (Ameloot et al., 1984) and unsaturated (Mitchell and Litman, 1998; Straume and Litman, 1987) lipids using time-dependent fluorescence anisotropy measurements. Thus, the DPH position in the lipid membrane is well understood, but its alignment with lipid molecules is still puzzling.

The MD simulations of the **ITZ/DPH-POPC** system show that the presence of ITZ significantly influenced the behavior of the DPH probe. First, the probe was pushed deeper into the bilayer and located below the ITZ molecules (Fig. 5). The mass density profile for DPH is broad with the maximum at ca. 0.34 nm. The longer DPH lifetimes measured in the ITZ-doped POPC membrane also suggests the deeper location of the probe in the POPC/ITZ bilayer. Second, the probe changed its orientation from parallel to predominantly perpendicular to the bilayer normal (Fig. 6). These changes are induced by the drug molecules, which are located close to the hydrophobic chain-headgroup interface. The ITZ molecules are relatively rigid and long, and adopt the orientation parallel to the membrane surface and impose a similar orientation on the probe. For this reason, the probe behavior does not reflect the lipid chain orientation anymore, but the orientation of the drug molecule. The effect of additives on the position of DPH in the lipid membrane has been studied for Chol (Kaiser and London, 1998). It was shown that the presence of 33 mol% Chol causes the probe molecules to move towards the center of the bilayer (0.67 nm from the membrane center). However, an impact of additives on the DPH orientation has not been studied.

5. Conclusions

We performed a comprehensive computational and experimental analysis of the behavior of DPH, a commonly used probe, in the zwitterionic bilayer with an admixture of the hydrophobic drug (ITZ), to evaluate its usefulness as a fluidity and microviscosity reporter for biomembranes treated with bioactive substances. Using this approach, we obtained a molecular insight into the organization of the membrane containing both DPH and ITZ. Our results showed that ITZ molecules tend to localize below the lipid headgroups and slightly above the lipid double bonds and orient perpendicular to the lipids. Therefore, the presence of the drug in the most rigid and ordered part of the membrane increased significantly the order of the upper segments of the acyl chains and concomitantly moved away the lipid molecules from each other. As a result, the free volume of the central region of the membrane considerably increases. The probe itself has a negligible impact on the structural properties of the lipid membrane. However, DPH induced the ordering of the entire lipid tails after insertion into the drug-containing membrane. This is the result of a deeper position of DPH and its orientation perpendicular to the lipids of DPH in the ITZ-doped membrane.

In summary, DPH is a very attractive rotational probe used commonly to characterize ordering, microviscosity and packing of lipid or cellular membranes. However, our results showed that DPH fluorescence anisotropy measurements might fail to predict the ordering, and packing of the lipid bilayer doped with drug molecules, as the location and orientation of DPH can be affected by the presence of molecules other than lipids in the bilayer in particular large, rigid, amphipathic molecules, which orient themselves parallel to the membrane surface. Thus, the use of DPH in systems with additives requires cautious in the interpretation of the fluorescence anisotropy data considering the potential effects of the additives on the behavior of DPH.

Transparency document

The Transparency document associated with this article can be found in the online version.

Acknowledgments

We thank the CSC-IT Centre for Science (Espoo, Finland) for excellent computational resources. For financial support, we thank the Academy of Finland (the Center of Excellence in Biomembrane Research – C.P., T.R.) and the European Research Council (Advanced Grant CROWDED-PRO-LIPIDS – C.P., T.R.). N.W. acknowledges the National Science Centre, Poland (NCN) for financial support in the form of ETIUDA doctoral scholarship on the basis of the decision number DEC-2017/24/T/ST5/00383.

Appendix A. Supplementary data

Supplementary material related to this article can be found, in the online version, at doi:https://doi.org/10.1016/j.chemphyslip.2019.104784.

References

Alves, A.C., Ribeiro, D., Horta, M., Lima, J.L.F.C., Nunes, C., Reis, S., 2017. The daunorubicin interplay with mimetic model membranes of cancer cells: a biophysical interpretation. Biochim. Biophys. Acta Biomembr. 1859, 941–948. https://doi.org/10.1016/j.bbamem.2017.01.034.

Ameloot, M., Hendrickx, H., Herreman, W., Pottel, H., Van Cauwelaert, F., van der Meer, W., 1984. Effect of orientational order on the decay of the fluorescence anisotropy in membrane suspensions. Experimental verification on unilamellar vesicles and lipid/alpha-lactalbumin complexes. Biophys. J. 46, 525–539. https://doi.org/10.1016/S0006-3495(84)84050-3.

Balducci, V., Incerpi, S., Stano, P., Tofani, D., 2018. Antioxidant activity of hydroxytyrosyl esters studied in liposome models. Biochim. Biophys. Acta Biomembr. 1860, 600–610. https://doi.org/10.1016/j.bbamem.2017.11.012.

Brejchová, J., Sýkora, J., Ostašov, P., Merta, L., Roubalová, L., Janáček, J., Hof, M., Svoboda, P., 2015. TRH-receptor mobility and function in intact and cholesterol-depleted plasma membrane of HEK293 cells stably expressing TRH-R-eGFP. Biochim. Biophys. Acta Biomembr. 1848, 781–796. https://doi.org/10.1016/j.bbamem.2014.11.029.

Bui, T.T., Suga, K., Umakoshi, H., 2016. Roles of sterol derivatives in regulating the properties of phospholipid bilayer systems. Langmuir 32, 6176–6184. https://doi.org/10.1021/acs.langmuir.5b04343.

Bussi, G., Donadio, D., Parrinello, M., 2007. Canonical sampling through velocity rescaling. J. Chem. Phys. 126, 014101. https://doi.org/10.1063/1.2408420.

Cerecedo, D., Martínez-Vieyra, I., Sosa-Peinado, A., Cornejo-Garrido, J., Ordaz-Pichardo, C., Benítez-Cardoza, C., 2016. Alterations in plasma membrane promote over-expression and increase of sodium influx through epithelial sodium channel in hypertensive platelets. Biochim. Biophys. Acta Biomembr. 1858, 1891–1903. https://doi.org/10.1016/j.bbamem.2016.04.015.

Clissold, S.M., Grant, S.P., 1989. Itraconazole a review of its pharmacodynamic and pharmacokinetic properties, and therapeutic use in superficial and systemic mycoses. Drugs 37, 310–344.

Darden, T., York, D., Pedersen, L., 1993. Particle mesh Ewald: an N· log(*N*) method for Ewald sums in large systems. J. Chem. Phys. 98, 10089–10092. https://doi.org/10.1063/1.464397.

De Athayde, Moncorvo, Collado, A., Dupuy, F.G., Morero, R.D., Minahk, C., 2016. Cholesterol induces surface localization of polyphenols in model membranes thus enhancing vesicle stability against lysozyme, but reduces protection of distant double bonds from reactive-oxygen species. Biochim. Biophys. Acta Biomembr. 1858, 1479–1487. https://doi.org/10.1016/j.bbamem.2016.04.002.

Demchenko, A.P., Mély, Y., Duportail, G., Klymchenko, A.S., 2009. Monitoring biophysical properties of lipid membranes by environment-sensitive fluorescent probes. Biophys. J. 96, 3461–3470. https://doi.org/10.1016/j.bpj.2009.02.012.

Dimova, R., 2019. Giant vesicles and their use in assays for assessing membrane phase state, curvature, mechanics and electrical properties. Annu. Rev. Biophys. 48, 93–119. https://doi.org/10.1146/annurev-biophys-052118-115342.

do Canto, A.M.T.M., Robalo, J.R., Santos, P.D., Carvalho, A.J.P., Ramalho, J.P.P., Loura, L.M.S., 2016. Diphenylhexatriene membrane probes DPH and TMA-DPH: a comparative molecular dynamics simulation study. Biochim. Biophys. Acta Biomembr. 1858, 2647–2661. https://doi.org/10.1016/j.bbamem.2016.07.013.

dos Santos, A.G., Bayiha, J.C., Dufour, G., Cataldo, D., Evrard, B., Silva, L.C., Deleu, M., Mingeot-Leclercq, M.P., 2017. Changes in membrane biophysical properties induced by the Budesonide/Hydroxypropyl-β-cyclodextrin complex. Biochim. Biophys. Acta Biomembr. 1859, 1930–1940. https://doi.org/10.1016/j.bbamem.2017.06.010.

Dzieciuch-Rojek, M., Poojari, C., Bednar, J., Bunker, A., Kozik, B., Nowakowska, M., Vattulainen, I., Wydro, P., Kepczynski, M., Róg, T., 2017. Effects of membrane PEGylation on entry and location of antifungal drug itraconazole and their pharmacological implications. Mol. Pharm. 14, 1057–1070. https://doi.org/10.1021/acs.molpharmaceut.6b00969.

Essmann, U., Perera, L., Berkowitz, M.L., Darden, T., Lee, H., Pedersen, L.G., 1995. A smooth particle mesh Ewald method. J. Chem. Phys. 103, 8577–8593. https://doi.org/10.1063/1.470117.

Faller, R., 2016. Molecular modeling of lipid probes and their influence on the membrane. Biochim. Biophys. Acta Biomembr. 1858, 2353–2361. https://doi.org/10.1016/j.bbamem.2016.02.014.

Filipe, H.A.L., Moreno, M.J., Róg, T., Vattulainen, I., Loura, L.M.S., 2014. How to tackle the issues in free energy simulations of long amphiphiles interacting with lipid membranes: convergence and local membrane deformations. J. Phys. Chem. B 118, 3572–3581. https://doi.org/10.1021/jp501622d.

Filippov, A., Orädd, G., Lindblom, G., 2003. The effect of cholesterol on the lateral diffusion of phospholipids in oriented bilayers. Biophys. J. 84, 3079–3086.

Fiorini, R., Valentino, M., Wang, S., Glaser, M., Gratton, E., 1987. Fluorescence lifetime distributions of 1,6-Diphenyl-1,3,5-hexatriene in Phospholipid Vesicles. Biochemistry 26, 3864–3870. https://doi.org/10.1021/bi00387a019.

Fraňová, M., Repáková, J., Čapková, P., Holopainen, J.M., Vattulainen, L., 2010. Effects of DPH on DPPC-Cholesterol membranes with varying concentrations of cholesterol: from local perturbations to limitations in fluorescence anisotropy experiments. J. Phys. Chem. B 114, 2704–2711. https://doi.org/10.1021/jp908533x.

García-Linares, S., Palacios-Ortega, J., Yasuda, T., Åstrand, M., Gavilanes, J.G., Martínez-Del-Pozo, Á., Slotte, J.P., 2016. Toxin-induced pore formation is hindered by intermolecular hydrogen bonding in sphingomyelin bilayers. Biochim. Biophys. Acta Biomembr. 1858, 1189–1195. https://doi.org/10.1016/j.bbamem.2016.03.013.

Giudice, F., Ambroggio, E.E., Mottola, M., Fanani, M.L., 2016. The amphiphilic alkyl ester derivatives of L-ascorbic acid induce reorganization of phospholipid vesicles. Biochim. Biophys. Acta Biomembr. 1858, 2132–2139. https://doi.org/10.1016/j.bbamem.2016.06.015.

Gomes, B., Gonçalves, S., Disalvo, A., Hollmann, A., Santos, N.C., 2018. Effect of 25-hydroxycholesterol in viral membrane fusion: insights on HIV inhibition. Biochim. Biophys. Acta Biomembr. 1860, 1171–1178. https://doi.org/10.1016/j.bbamem.2018.02.001.

Hess, B., Bekker, H., Berendsen, H.J.C., Fraaije, J.G.E.M., 1997. LINCS: a linear constraint solver for molecular simulations. J. Comput. Chem. 18, 1463–1472. https://doi.org/10.1002/(SICI)1096-987X(199709)18:12<1463::AID-JCC4>3.0.CO;2-H.

Jorgensen, W.L., Chandrasekhar, J., Madura, J.D., Impey, R.W., Klein, M.L., 1983. Comparison of simple potential functions for simulating liquid water. J. Chem. Phys. 79, 926–935. https://doi.org/10.1063/1.445869.

Kaiser, R.D., London, E., 1998. Location of diphenylhexatriene (DPH) and its derivatives within membranes: comparison of different fluorescence quenching analyses of membrane depth. Biochemistry 37, 8180–8190. https://doi.org/10.1021/bi980064a.

Kaminski, G.A., Friesner, R.A., Tirado-Rives, J., Jorgensen, W.L., 2001. Evaluation and reparametrization of the OPLS-AA force field for proteins via comparison with accurate quantum chemical calculations on peptides. J. Phys. Chem. B 105, 6474–6487. https://doi.org/10.1021/jp003919d.

Kang, M., Day, C.A., Kenworthy, A.K., DiBenedetto, E., 2012. Simplified equation to extract diffusion coefficients from confocal FRAP data. Traffic 13, 1589–1600. https://doi.org/10.1111/tra.12008.

Kepczynski, M., Kumorek, M., Stepniewski, M., Róg, T., Kozik, B., Jamróz, D., Bednar, J., Nowakowska, M., 2010. Behavior of 2,6-Bis(decyloxy)naphthalene inside lipid bilayer. J. Phys. Chem. B 114. https://doi.org/10.1021/jp103753f.

Kepczynski, M., Lewandowska, J., Witkowska, K., Kędracka-Krok, S., Mistrikova, V., Bednar, J., Wydro, P., Nowakowska, M., 2011. Bilayer structures in dioctadecyldimethylammonium bromide/oleic acid dispersions. Chem. Phys. Lipids 164, 359–367. https://doi.org/10.1016/j.chemphyslip.2011.04.007.

Kepczyński, M., Nawalany, K., Kumorek, M., Kobierska, A., Jachimska, B., Nowakowska, M., 2008. Which physical and structural factors of liposome carriers control their drug-loading efficiency? Chem. Phys. Lipids 155, 7–15. https://doi.org/10.1016/j.chemphyslip.2008.05.174.

Kepczynski, M., Róg, T., 2016. Functionalized lipids and surfactants for specific applications. Biochim. Biophys. Acta Biomembr. 1858, 2362–2379. https://doi.org/10.1016/j.bbamem.2016.02.038.

Klymchenko, A.S., Kreder, R., 2014. Fluorescent probes for lipid rafts: from model membranes to living cells. Chem. Biol. 21, 97–113. https://doi.org/10.1016/j.chembiol.2013.11.009.

König, B., Dietrich, U., Klose, G., 1997. Hydration and structural properties of mixed Lipid/Surfactant model membranes. Langmuir 13, 525–532. https://doi.org/10.1021/la960571y.

Kulig, W., Jurkiewicz, P., Olzyńska, A., Tynkkynen, J., Javanainen, M., Manna, M., Róg, T., Hof, M., Vattulainen, I., Jungwirth, P., 2015a. Experimental determination and computational interpretation of biophysical properties of lipid bilayers enriched by cholesteryl hemisuccinate. Biochim. Biophys. Acta Biomembr. 1848, 422–432. https://doi.org/10.1016/j.bbamem.2014.10.032.

Kulig, W., Olzyńska, A., Jurkiewicz, P., Kantola, A.M., Komulainen, S., Manna, M., Pourmousa, M., Vazdar, M., Cwiklik, L., Róg, T., Khelashvili, G., Harries, D., Telkki, V.V., Hof, M., Vattulainen, I., Jungwirth, P., 2015b. Cholesterol under oxidative stress - how lipid membranes sense oxidation as cholesterol is being replaced by oxysterols. Free Radic. Biol. Med. 84, 30–41. https://doi.org/10.1016/j.freeradbiomed.2015.03.006.

Kulig, W., Pasenkiewicz-Gierula, M., Róg, T., 2015c. Topologies, structures and parameter files for lipid simulations in GROMACS with the OPLS-aa force field: DPPC, POPC, DOPC, PEPC, and cholesterol. Data Br. 5, 333–336. https://doi.org/10.1016/j.dib.2015.09.013.

Kulig, W., Pasenkiewicz-Gierula, M., Róg, T., Róg, T., 2016. Cis and trans unsaturated phosphatidylcholine bilayers: a molecular dynamics simulation study. Chem. Phys. Lipids 195, 12–20. https://doi.org/10.1016/j.chemphyslip.2015.07.002.

Lakowicz, J.R., 2006. Principles of Fluorescence Spectroscopy, 3rd ed. Springer, US. https://doi.org/10.1007/978-0-387-46312-4.

Lira, R.B., Dimova, R., Riske, K.A., 2014. Giant unilamellar vesicles formed by hybrid films of agarose and lipids display altered mechanical properties. Biophys. J. 107, 1609–1619. https://doi.org/10.1016/j.bpj.2014.08.009.

Lira, R.B., Steinkühler, J., Knorr, R.L., Dimova, R., Riske, K.A., 2016. Posing for a picture: vesicle immobilization in agarose gel. Sci. Rep. 6, 1–12. https://doi.org/10.1038/srep25254.

Maciejewski, A., Pasenkiewicz-Gierula, M., Cramariuc, O., Vattulainen, I., Róg, T., 2014. Refined OPLS-AA force field for saturated phosphatidylcholine bilayers at full hydration. J. Phys. Chem. B 118, 4571–4581. https://doi.org/10.1021/jp5016627.

Mason, R.P., Jacob, R.F., Shrivastava, S., Sherratt, S.C.R., Chattopadhyay, A., 2016. Eicosapentaenoic acid reduces membrane fluidity, inhibits cholesterol domain formation, and normalizes bilayer width in atherosclerotic-like model membranes. Biochim. Biophys. Acta Biomembr. 1858, 3131–3140. https://doi.org/10.1016/j.bbamem.2016.10.002.

Melikishvili, S., Poturnayova, A., Ionov, M., Bryszewska, M., Vary, T., Cirak, J., Muñoz-Fernández, M.Á., Gomez-Ramirez, R., de la Mata, F.J., Hianik, T., 2016. The effect of polyethylene glycol-modified lipids on the interaction of HIV-1 derived peptide–-dendrimer complexes with lipid membranes. Biochim. Biophys. Acta Biomembr. 1858, 3005–3016. https://doi.org/10.1016/j.bbamem.2016.09.005.

Miguel, V., Sánchez-Borzone, M.E., García, D.A., 2018. Interaction of gabaergic ketones with model membranes: a molecular dynamics and experimental approach. Biochim. Biophys. Acta Biomembr. 1860, 1563–1570. https://doi.org/10.1016/j.bbamem.2018.05.012.

Mitchell, D.C., Litman, B.J., 1998. Molecular order and dynamics in bilayers consisting of highly polyunsaturated phospholipids. Biophys. J. 74, 879–891. https://doi.org/10.1016/S0006-3495(98)74011-1.

Mobarak, E., Javanainen, M., Kulig, W., Honigmann, A., Sezgin, E., Aho, N., Eggeling, C., Rog, T., Vattulainen, I., 2018. How to minimize dye-induced perturbations while studying biomembrane structure and dynamics: PEG linkers as a rational alternative. Biochim. Biophys. Acta Biomembr. https://doi.org/10.1016/j.bbamem.2018.07.003.

Neves, A.R., Nunes, C., Reis, S., 2016. Resveratrol induces ordered domains formation in biomembranes: implication for its pleiotropic action. Biochim. Biophys. Acta Biomembr. 1858, 12–18. https://doi.org/10.1016/j.bbamem.2015.10.005.

Neves, A.R., Nunes, C., Reis, S., 2015. New insights on the biophysical interaction of resveratrol with biomembrane models: relevance for its biological effects. J. Phys. Chem. B 119, 11664–11672. https://doi.org/10.1021/acs.jpcb.5b05419.

Pandey, B.N., Mishra, K.P., 1999. Radiation induced oxidative damage modification by cholesterol in liposomal membrane. Radiat. Phys. Chem. 54, 481–489.

Parrinello, M., Rahman, A., 1981. Polymorphic transitions in single crystals: a new molecular dynamics method. J. Appl. Phys. 52, 7182–7190. https://doi.org/10.1063/1.328693.

Pirc, K., Ulrih, N.P., 2015. α-Synuclein interactions with phospholipid model membranes: key roles for electrostatic interactions and lipid-bilayer structure. Biochim. Biophys. Acta Biomembr. 1848, 2002–2012. https://doi.org/10.1016/j.bbamem.2015.06.021.

Pronk, S., Páll, S., Schulz, R., Larsson, P., Bjelkmar, P., Apostolov, R., Shirts, M.R., Smith, J.C., Kasson, P.M., Van Der Spoel, D., Hess, B., Lindahl, E., 2013. GROMACS 4.5: a high-throughput and highly parallel open source molecular simulation toolkit. Bioinformatics 29, 845–854. https://doi.org/10.1093/bioinformatics/btt055.

Repáková, J., Čapková, P., Holopainen, J.M., Vattulainen, I., 2004. Distribution, orientation, and dynamics of DPH probes in DPPC bilayer. J. Phys. Chem. B. https://

doi.org/10.1021/jp048381g.
Repáková, J., Holopainen, J.M., Morrow, M.R., McDonald, M.C., Čapková, P., Vattulainen, I., 2005. Influence of DPH on the structure and dynamics of a DPPC bilayer. Biophys. J. 88, 3398–3410. https://doi.org/10.1529/biophysj.104.055533.
Stepniewski, M., Kepczynski, M., Jamróz, D., Nowakowska, M., Rissanen, S., Vattulainen, I., Róg, T., 2012. Interaction of hematoporphyrin with lipid membranes. J. Phys. Chem. B 116, 4889–4897. https://doi.org/10.1021/jp300899b.
Straume, M., Litman, B.J., 1987. Equilibrium and Dynamic Structure of Large, Unilamellar, Unsaturated Acyl Chain Phosphatidylcholine Vesicles. Higher Order Analysis of 1,6-Diphenyl-1,3,5-hexatriene and 1 -[4-(Trimethylammonio)phenyl]-6-phenyl-1,3,5-hexatriene Anisotropy Decay. Biochemistry 26, 5113–5120. https://doi.org/10.1021/bi00390a033.
Suzuki, M., Miura, T., 2015. Effect of amyloid β-peptide on the fluidity of phosphatidylcholine membranes: uses and limitations of diphenylhexatriene fluorescence anisotropy. Biochim. Biophys. Acta Biomembr. 1848, 753–759. https://doi.org/10.1016/j.bbamem.2014.12.003.
Timr, Š., Brabec, J., Bondar, A., Ryba, T., Železný, M., Lazar, J., Jungwirth, P., 2015. Nonlinear optical properties of fluorescent dyes allow for accurate determination of their molecular orientations in phospholipid membranes. J. Phys. Chem. B 119, 9706–9716. https://doi.org/10.1021/acs.jpcb.5b05123.
Vaňousová, K., Beranová, J., Fišer, R., Jemioła-Rzemińska, M., Matyska Lišková, P., Cybulski, L., Strzałka, K., Konopásek, I., 2018. Membrane fluidization by alcohols inhibits DesK-DesR signalling in Bacillus subtilis. Biochim. Biophys. Acta Biomembr. 1860, 718–727. https://doi.org/10.1016/j.bbamem.2017.12.015.
Wang, L.H., Wang, M.S., Zeng, X.A., Liu, Z.W., 2016. Temperature-mediated variations in cellular membrane fatty acid composition of Staphylococcus aureus in resistance to pulsed electric fields. Biochim. Biophys. Acta Biomembr. 1858, 1791–1800. https://doi.org/10.1016/j.bbamem.2016.05.003.
Wang, L.H., Zeng, X.A., Wang, M.S., Brennan, C.S., Gong, D., 2018. Modification of membrane properties and fatty acids biosynthesis-related genes in Escherichia coli and Staphylococcus aureus: implications for the antibacterial mechanism of naringenin. Biochim. Biophys. Acta Biomembr. 1860, 481–490. https://doi.org/10.1016/j.bbamem.2017.11.007.
Yun, D.G., Lee, D.G., 2017. Silymarin exerts antifungal effects via membrane-targeted mode of action by increasing permeability and inducing oxidative stress. Biochim. Biophys. Acta Biomembr. 1859, 467–474. https://doi.org/10.1016/j.bbamem.2017.01.009.
Yun, J., Lee, H., Ko, H.J., Woo, E.R., Lee, D.G., 2015. Fungicidal effect of isoquercitrin via inducing membrane disturbance. Biochim. Biophys. Acta Biomembr. 1848, 695–701. https://doi.org/10.1016/j.bbamem.2014.11.019.
Yun, J.E., Woo, E.R., Lee, D.G., 2018. Effect of isoquercitrin on membrane dynamics and apoptosis-like death in Escherichia coli. Biochim. Biophys. Acta Biomembr. 1860, 357–363. https://doi.org/10.1016/j.bbamem.2017.11.008.
Zannoni, C., Arcioni, A., Cavatorta, P., 1983. Fluorescence depolarization in liquid crystals and membrane bilayers. Chem. Phys. Lipids 32, 179–250. https://doi.org/10.1016/0009-3084(83)90037-3.